Received: 12 October 2023 | Revised: 15 May 2024 | Accepted: 29 June 2024

DOI: 10.1002/joc.8559

RESEARCH ARTICLE

International Journal of Climatology RMetS

Future change of humid heat extremes and population exposure in Turkey

Berkay Donmez | **Kutay Donmez** | **Cemre Yürük Sonuç** | **Yurdanur Unal**

Department of Meteorological Engineering, Faculty of Aeronautics and Astronautics, Istanbul Technical University, Istanbul, Turkey

Correspondence
Berkay Donmez, Extreme Environments Research Laboratory, École Polytechnique Fédérale de Lausanne (EPFL) Valais Wallis, Sion, Switzerland.
Email: berkay.donmez@epfl.ch

Present addresses
Kutay Donmez, Extreme Environments Research Laboratory, École Polytechnique Fédérale de Lausanne (EPFL) Valais Wallis, Sion, Switzerland; Department of Environmental Systems Science, ETH Zurich, Zurich, Switzerland; Laboratory of Atmospheric Processes and their Impacts, Ecole Polytechnique Fédérale de Lausanne, Lausanne, Switzerland; and Laboratory for Air Pollution/ Environmental Technology, Empa, Dübendorf, Switzerland.

Funding information
TUBITAK, Grant/Award Number: 114Y047

Abstract

Global climate projections show that humid heat extremes will expand toward the higher latitudes, making the midlatitudes hotspots for these extremes. Therefore, a thorough explanation of their regional characteristics becomes crucial, given that the changes in these extremes can potentially render a large proportion of the global population at risk. Here, we perform the first analysis of historical and projected changes in the intensity and frequency of humid heat extremes and quantify the population exposure to these extremes in Turkey, using long-term simulations from the non-hydrostatic mesoscale model of Consortium for Small-scale Modeling (COSMO-CLM) under the RCP8.5 emission scenario. We portray not only the nationwide changes in the humid heat extremes and population exposure but also their regional aspects by exploiting the *K*-means clustering algorithm. Our results suggest significant future increases in the intensity and frequency of these extremes over a wide geographical area, which includes the surroundings of Adana, Antalya, Izmir, Sakarya, Ordu and Diyarbakir, most of which are coastal locations. Over most of these regions, severe humid heat stress is expected to last nearly a month every year, with almost 56% of the land area is projected to experience local historical upper tail heat stress conditions for at least an additional 10 consecutive hours. Further, we explicate a significant rise in the number of people exposed to severe humid heat stress, concentrated along most coastal regions, by as much as 1.6 million person-days. More than 20% of Turkey's population may confront severe humid heat stress for at least 1 h, with that percentage falling to 4.15% for at least five consecutive hours, which indicates that people will not only endure more intense humid heat stress but also be exposed to these conditions consecutively over a period of many hours.

KEYWORDS

heat stress, population exposure, regional climate change, Turkey

1 | INTRODUCTION

Previous studies indicate that extreme temperature periods in populated regions can be life-threatening. At this point, the observed and projected increase in the intensity and frequency of extreme heat events worldwide renders quantitative and qualitative assessments of the impact of these extremes on human well-being crucially important. This involves factoring in the multidimensional, likely sequential, and lasting footprint of the changing climate on society encompassing areas such as social life, tourism and economy (Gasper et al., 2011). The heat stress term has been commonly used in the literature to address the potential impact of heat extremes, both dry and humid heat, on human physiology. Though some studies utilized dry heat metrics (e.g., temperature) in their studies, expressing heat stress through a combination of temperature and humidity can enhance the understanding of the physical interaction between the human body and thermal stress (i.e., humid heat stress; Mishra et al., 2020). These two variables, when used simultaneously, were shown to be the most accurate in detecting past deadly and non-deadly heat episodes (Mora et al., 2017). Essentially, the heat produced internally in a human body is subject to thermoregulation, and the efficiency of the body's ability to thermoregulate itself is strongly linked to the temperature gradient between the body and the air surrounding it (Sherwood & Huber, 2010). The narrower this gradient becomes, the more difficult it is for humans to cool down through sweating, which increases the risk of morbidity and mortality. For example, Sherwood and Huber (2010) argue that a wet-bulb temperature gradient of 1–2°C is required for efficient internal heat release when using the wet-bulb temperature to express humid heat stress.

Given the interaction between temperature and humidity that is nonlinear and not straightforward to unravel, a variety of heat stress indices are employed in the scientific community to study heat stress. Some of the most commonly used metrics are the wet-bulb temperature, wet-bulb globe temperature, heat index and apparent temperature, each of which has unique features and assumptions, such as its physical constraints and relationship to critical meteorological variables (i.e., insolation and wind speed) as well as clothing and metabolical processes for humans. Among these indices, the wet-bulb temperature is not only comparatively more sensitive to humidity but also more resistant to hotter climates (Sherwood, 2018), making it a relevant and popularly adapted metric for studies that systematically consider the impact of a changing climate on the local and global patterns and extremes of humid heat (Freychet et al., 2022; Raymond et al., 2020). Further, it provides a theoretical benchmark for assessing physiological impacts, as it is well-established that humans are unlikely to survive exposure to wet-bulb temperatures above 35°C, even with adaptation measures (Sherwood & Huber, 2010). Interestingly, mortality risk due to heat stress below this value (i.e., 35°C) is still not unlikely, as revealed by past heat events (Mazdiyasni et al., 2017; Raymond et al., 2020).

Studies explicate the importance of utilizing more than one metric in the assessment of humid heat extremes (Freychet et al., 2022; Tuholske et al., 2021). However, regardless of the employed indices that synergically combine temperature and humidity, extremes of these indices in a changing climate pose further intensification, along with an increase in their frequency and duration (Freychet et al., 2022; Raymond et al., 2020; Wang et al., 2021; Wu et al., 2014). A recent synthesis of the extreme wet-bulb temperatures already reveals that the deadly threshold of 35°C has been experienced in some locations, and the exceedance of this critical value over land can become a regular occurrence with climate change (Chen et al., 2022; Raymond et al., 2020). Potential increases in the frequency of these extremes are further consequential, given the higher risks of mortality associated with a rise in frequency rather than the severity of events (Ahmadalipour et al., 2019). Such increases in the humid heat intensity and return period values are noteworthy. Historically, wet-bulb temperature values surpassing 35°C were only present during the Paleogene period (Sherwood & Huber, 2010).

The land area already subject to humid heat extremes will experience dramatic increases in the frequency and intensity of these extremes (Matthews et al., 2017). These hotspots include a geographically wide area across the tropics and the coastal Middle East (Freychet et al., 2022; Raymond et al., 2020). Studies give particular emphasis to these regions, as they are likely to be regularly exposed to threatening wet-bulb temperature values (e.g., 27–31°C), with frequencies ranging from 5 to 50 days per year (Coffel et al., 2019; Freychet et al., 2022). On the other hand, heat stress extremes currently confined to the tropics and subtropics will expand toward higher latitudes with global warming. This expansion will be less pronounced in the Southern Hemisphere (Freychet et al., 2022; Matthews et al., 2017; Wang et al., 2021), making the midlatitudes the hotspots for intensified heat stress extremes (Fischer & Knutti, 2013; Mora et al., 2017; Wang et al., 2021). Thus, owing to the geographical dependence of these extremes (Raymond et al., 2021), it is critically important to present an elaborate demonstration of their regional characteristics.

Quantifying population exposure to heat stress has been an inevitable part of the risk and vulnerability assessments. Literature elucidates that humid heat extremes impact regions with dense populations, ascertaining the need for exposure analyses at the country and city levels (Russo et al., 2017). A standard way to define exposure is by employing the person-days approach, which formulates the exposure as the number of people in a region times the number of days per year experiencing certain heat stress conditions (i.e., a heat index value above a specified threshold). While the number of people exposed to these extremes varies from one region to another, there has been a dramatic increase in global exposure to these extremes (Mora et al., 2017; Sherwood & Huber, 2010; Tuholske et al., 2021). A study quantified this increasing trend as 199% from 1983 to 2016 (Tuholske et al., 2021), and another one showed that almost one-third of the world population was exposed to deadly heat stress in 2000 (Mora et al., 2017), though it is likely that this number would be higher today.

Business-as-usual projections of global exposure are demonstrated that approximately 75% of the world population will be at risk of exposure to severe heat stress by the end of this century (Mora et al., 2017). A recent study quantifying exposure at different warming levels plotted a scenario that with a 3.0°C increase in global mean temperatures, up to 5 billion people could be regularly exposed to wet-bulb temperatures above 27.5°C, leading severe heat stress, and up to 100 million people could experience the deadly wet-bulb temperature threshold of 35°C (Freychet et al., 2022). It should be noted that regardless of the employed warming scenario or metric, studies agree that increases in population exposure to heat stress are significant (Chen et al., 2022; Freychet et al., 2022; Mora et al., 2017; Rothfusz, 1990; Sherwood & Huber, 2010). For example, the findings of Freychet et al. (2022) reveal that the increase in population exposure with increasing global warming levels is consistent both in terms of magnitude and area impacted when the metrics of wet-bulb temperature, wet-bulb globe temperature and heat index are used. Population exposure derived from each metric reiterates that densely populated areas are expected to bear the burden of more than one order of magnitude increase in exposure.

Countries in the Middle East, West Africa and South America, as well as China and the United States, are some of the regions exposed to dangerous combinations of temperature and humidity variables (Chen et al., 2022; Freychet et al., 2022; Jones et al., 2015). For example, shifting of the global mean temperature above pre-industrial levels from 1.5 to 3°C translates into 20% to 60% increase in exposure in humid heat stress hazard, rendering these regions as hotspot research areas (Freychet et al., 2022). Specifically, over the West Africa, the anticipated exposure to wet-bulb temperature above 27.5°C is within the prospects of reaching 80%, while only 10% of the population is affected by the value above 31°C. Moreover, under SSP5-8.5 scenario, the exposure to humid heat levels in China has the potential to influence as much as 81% of the population by 2100, which further translates into public health concern (Chen et al., 2022). Not only Asia but also Contiguous United States expects to encounter a rise in days with extreme heat, specifically along and across the southern portions of the country including Texas and its surroundings (Jones et al., 2015). Regional differences still exist, rendering the regional aspects of the exposure component highly relevant and critical.

Turkey's climate is also susceptible to change, with a remarkable increase in observed temperatures (Turkes & Sumer, 2004), and regional temperature values projected to reach as much as 5°C (Onol & Unal, 2014). Though Turkey is located in the Eastern Mediterranean region, which is experiencing increasing trends in humidity across its coastal regions (Onol et al., 2014) and climate extremes (Kelebek et al., 2021), and sharing a coast with the humid and hot-prone regions of the Middle East in the southeast (Raymond et al., 2020), no prior study to our knowledge has elaborated on the vulnerability aspect of the projected changes in the temperature extremes in Turkey, let alone combined temperature-humidity extremes. A study by Diffenbaugh et al. (2007), however, highlighted the preferential increase in projected heat stress across the Mediterranean coast, with more dangerous heat stress conditions already found over the eastern and southern Mediterranean in the reference period. Here for the first time, we reveal the present and projected changes in the intensity and frequency of humid heat extremes across the climatologically different regions of Turkey, quantify the number of people anticipated to confront these extremes, and demonstrate the regional differences in the exposure component.

2 | DATA AND METHODS

2.1 | Regional climate modelling

We simulate long-term continuous historical (1979–2005) and future (2024–2100) climates using the non-hydrostatic mesoscale atmospheric model of the Consortium for Small-scale Modeling (COSMO-CLM) developed by the CLM-Community of German Meteorological Service (DWD), and apply the Representative Concentration Pathways 8.5 (RCP8.5) emission scenario. The model is forced with the simulations provided by the earth system model of the Max Planck Institute for Meteorology

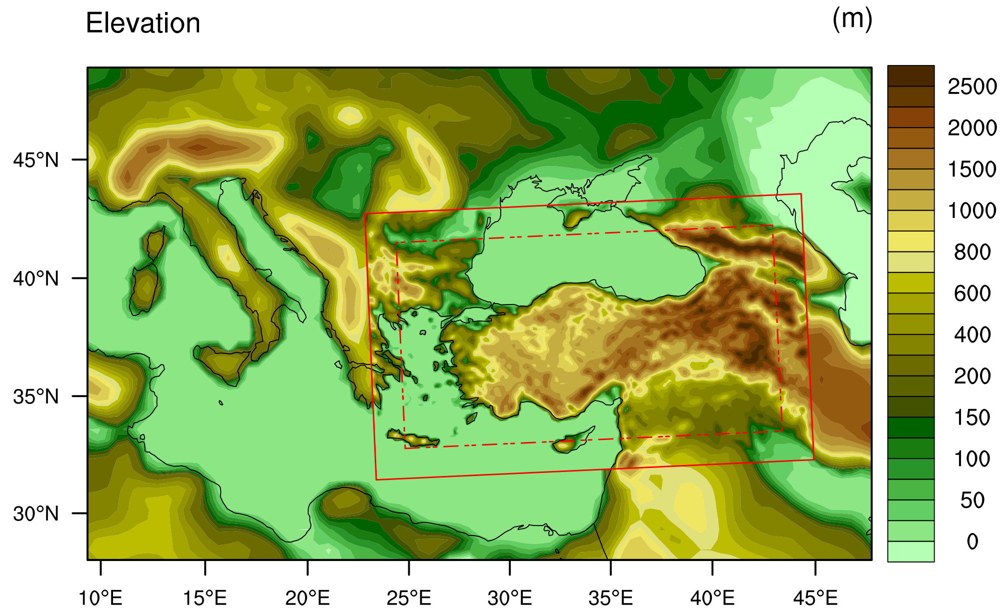

FIGURE 1 The COSMO-CLM model domains for the 0.44° (the larger domain) and 0.11° (the nested domain covered by dashed red lines) simulations. The region between the solid and dashed red lines represents the sponge zone, separated by 12 grid points.

(MPI-ESM-LR), a participant in the CMIP5 (Coupled Models Intercomparison Project Phase 5) collaboration. First, the global model simulations are dynamically downscaled to 0.44° resolution in a domain encompassing the majority of the Eastern Mediterranean region (Figure 1). Then, we further downscale the 0.44° climate simulations to 0.11° horizontal resolution over Turkey. The model equations were solved using the third-order two time-level Runge Kutta scheme in a terrain-following height-based hybrid Gal-Chen coordinate system. GLC2000 (Global Land Cover Map for the year 2000) data at 1 km resolution is preferred as land use data. We define 40 vertical levels in the atmosphere, and the number of soil levels is set to 9. Table 1 illustrates the overall model configuration and the parameterization schemes utilized to represent subgrid-scale processes.

2.2 | Humid heat stress metric

The heat stress metric used in our study is based on the popularly adopted wet-bulb temperature (WBT), considering its superiority to other metrics in terms of its robustness to climate change (Sherwood, 2018). We calculate hourly wet-bulb temperature from the model output as our humid heat stress metric and constrain the heat stress analysis to 20-year summertime periods, prioritizing the trends and changes in the last two decades of the historical period (i.e., 1985–2005) and projection period (2081–2100). The estimation of the WBT at an hourly interval facilitates focusing on the heat stress caution hours, a concept used for quantifying the number of hours humans are exposed to threatening heat stress conditions (Sarangi et al., 2021).

TABLE 1 The COSMO-CLM model configurations for the 0.44° and 0.11° domains.

Content	Domains	
Horizontal resolution	0.44°	0.11°
Grid cell	ie = 79, je = 50	ie = 175, je = 107
Vertical levels	40μ level	40μ level
Time interval	240 s	90 s
Microphysics scheme	2-category ice scheme	2-category ice scheme
Convection scheme	Tiedtke (1989)	Tiedtke (1989)
Radiation scheme	Ritter and Geleyn (1992)	Ritter and Geleyn (1992)
Vertical turbulent diffusion scheme	1-D TKE-based	1-D TKE-based
Surface transfer scheme	TKE-based	TKE-based
Land surface scheme	TERRA-ML	TERRA-ML
Periods: RF and RCP8.5	RF: 197908–200512 RCP: 202408–210012	RF: 198108–200512 RCP: 202608–210012

We employed the Stull (2011) version of the WBT formulation, which incorporates the essential heat stress variables of the air temperature (T) and relative humidity (RH),

$$\begin{aligned}\mathrm{WBT} = {} & T\,\mathrm{atan}\left[0.151977(\mathrm{RH\%}+8.313659)^{\frac{1}{2}}\right] \\ & + \mathrm{atan}(T+\mathrm{RH\%}) - \mathrm{atan}(\mathrm{RH\%}-1.676331) \\ & + 0.00391838(\mathrm{RH\%})^{\frac{3}{2}}\mathrm{atan}(0.023101\mathrm{RH\%}) \\ & - 4.686035. \end{aligned} \quad (1)$$

The validity of Equation (1) is constrained by the predefined ranges of the air temperature and RH (Stull, 2011). Namely, it operates for air temperatures between −20 and 50°C, and the RH from 5% up to 99%.

Unlike our climate model output, the RH variable is not available in the ERA5-Land reanalysis used here for verification purposes. Therefore, to calculate RH in ERA5-Land (Equations (2)–(4)), we utilized the available air (T) and dew-point temperature (T_d) variables,

$$\mathrm{RH}=100\%\times\frac{e(T)}{e_s(T)},\tag{2}$$

$$e=e_s0\times\exp\left(\frac{L_v}{R_v}\times\left(\frac{1}{T_0}-\frac{1}{T_d}\right)\right),\tag{3}$$

$$e_s=e_s0\times\exp\left(\frac{L_v}{R_v}\times\left(\frac{1}{T_0}-\frac{1}{T}\right)\right),\tag{4}$$

where e and e_s are vapour pressure and saturation vapour pressure, respectively. Here, L_v (i.e., latent heat of vaporization of water) is 2.501 × 106 J·kg^{-1} and R_v (i.e., gas constant for water vapour) is 461.5 J·K^{-1}. Further, although the climate model output contains a wet-bulb temperature variable, we calculated the WBT ourselves employing Equation (1) to enable a smooth comparison between the model WBT values and ERA5-Land WBT values.

We mainly utilize three different WBT thresholds, which are 27, 29 and 31°C, in our analysis. We refer to the former and the latter thresholds as severe humid heat stress and dangerous heat stress, respectively similar to Freychet et al. (2022).

2.3 | Verification and bias correction procedure

The summertime hourly WBT model output is bias-corrected and verified against the ERA5-Land reanalysis product for the historical and projected periods spanning 1985–2005 and 2081–2100. Recent studies have demonstrated the application of the bias-correction procedure directly on the WBT variable (Chen et al., 2022), instead of bias-correcting the individual components of the WBT (i.e., air temperature and RH), to successfully reduce the systematic biases inherent to the climate model and reproduce the overall characteristics of the variable. To this end, the summertime hourly WBT model outputs are bias-corrected using an empirical quantile mapping (EQM) approach for the historical period (1985–2005), and the computed correction factors are then applied to the projected hourly WBT values. EQM is a distribution-free correction method that maps the model output quantiles to the observed quantiles, considering several predetermined empirical quantiles. Here, we use 16 manually determined quantiles to approximate the empirical CDFs of the WBT from the ERA5-Land reanalysis and model output. Our implementation of EQM is based on the xclim Python package (Logan et al., 2023).

2.4 | Humid heat extremes metrics

Emphasizing the relative long-term changes in the extremes of the WBT series, we utilized the magnitude metrics of the yearly maximum (max) and 99th percentile (q99) of hourly WBT values for the respective study periods. On the other hand, we employed three different frequency metrics. These are the number of days in a year where the daily maximum WBT exceeds 27°C (severe humid heat stress; NOD27), the number of consecutive hours where the hourly WBT exceeds 27°C (NOCH27) and the number of consecutive hours where the hourly WBT is above the local q99 of the historical period (NOCHQ99).

2.5 | Population exposure definition

We quantified the population exposure to the WBT extremes by means of the widely exploited person-days approach, whereby we analysed the long-term changes in yearly population exposure during the reference and projected periods (Jones et al., 2015). Namely, this approach characterizes the exposure to the WBT extremes by multiplying the number of people by the number of days in a year when extreme WBT conditions occur. Therefore, our exposure definition considers the concurrent trends or changes in extreme heat stress conditions and population count. To isolate the relative contribution of the extreme heat stress to the exposure, we conducted an alternative exposure analysis in which we held the population count constant throughout the analysed period and vice versa. This allowed us to investigate the so-called population and climate components of the total population exposure.

To calculate the climate component of the total population exposure, we allow the climate to evolve during the projection period but keep the population data constant at the historical period levels. Similarly, calculating the population component requires allowing the population of Turkey to evolve during the projection period while the climate is kept at the average of the last 5 years of the historical period. We investigate these components only for nationwide analyses. The total population exposure is further aggregated to specific regions

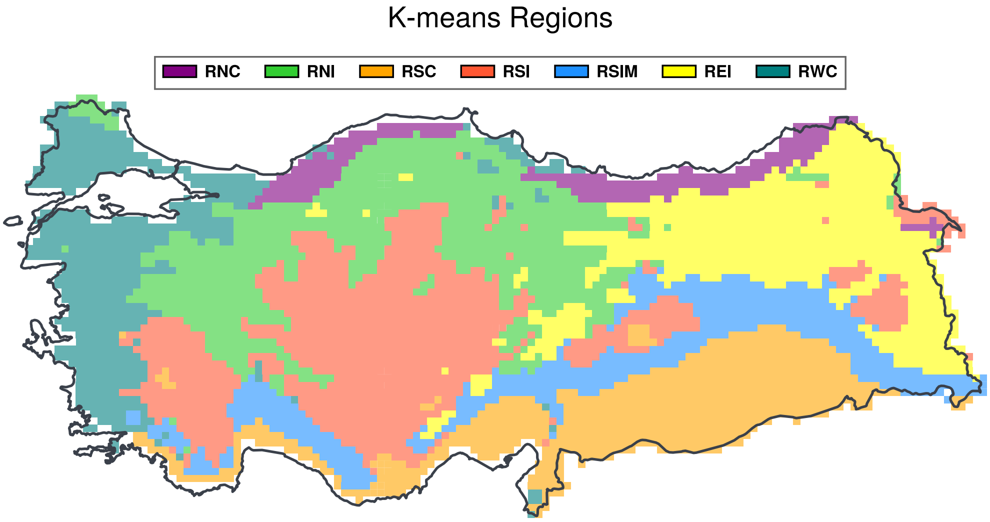

FIGURE 2 Conceptualized *K*-means regions across Turkey named according to their geographical location and proximity to water bodies.

conceptualized using a clustering algorithm, explained in the following section, allowing us to concentrate on the regional aspects of exposure.

For the reference period, we used the gridded population estimates from the Gridded Population of the World version 4 (GPWv4) data (CIESIN, 2018), and the future population estimates are based on the Shared Socioeconomic Pathways 5 (SSP5) scenario (Jones & O'Neill, 2020), considering its radiative similarity with the RCP8.5 scenario. Though the GPWv4 data consists of the global estimates of population count every 5 years between 2000 and 2015, we used the population count estimates for 2005 for the historical analysis in line with our historical (1985–2005) period. In contrast, the obtained SSP5 projection data covers the years 2081–2100 with a temporal resolution of 10 years. To calculate interannual changes in the exposure, we linearly interpolated the 10-yearly data and created yearly population time series for use in our exposure analysis.

We also regridded the population datasets to match the native grid of the climate model data. These datasets have a grid resolution of 2.5 arc min (∼5 km) and 7.5 arc min (∼10 km), slightly higher than our climate model grid. Therefore, we first coarsened the relatively higher resolution population datasets to approximately match the climate model grid resolution. This avoided significant information loss while remapping. Finally, we bilinearly interpolated the population data grid onto the climate model grid.

2.6 | *K*-means clustering algorithm

We employed the *K*-means clustering algorithm to conceptualize seven climatologically unique regions across Turkey, consistent with the traditional categorization of Turkey's geographical regions into seven distinct areas. The clustering of these regions is based on the hourly 2-m temperature, 2-m RH and total precipitation model outputs aggregated to seasonal values for each season in a year and averaged across the historical period. For this purpose, we used the *K*-means algorithm, and the computations are made using Lloyd's algorithm. Overall, the *K*-means algorithm aims to cluster data points whose distance to a centroid is minimized. The clustered regions are shown in Figure 2.

For brevity, these regions are named according to their geographical location and proximity to water bodies, which we elaborate on in the results section (Table 1). For example, the region constrained to the western coast of the country is referred to as RWC (i.e., Region West Coastal). The naming convention, along with the population statistics (i.e., population percentage and projected changes) for each of these conceptualized regions, are given in Table 2. The regions RWC and RSC constitute the biggest shares of the total population in the country, with corresponding percentages of 21.41% and 25.60%. About 17% of the total population resides in both the regions RSI and RNI, while the remaining *K*-means regions combined make up less than 20% of the total population. These regions are used throughout the study, complementary to the nationwide analyses, particularly while analysing population exposure to the humid heat extremes.

3 | RESULTS

3.1 | Model verification

We verify the seasonally aggregated extreme and median WBT values derived from the hourly 2 m temperature

TABLE 2 The region names used throughout the study, along with the share of the population and the projected population changes, for conceptualized *K*-means regions.

Statistics	Reg. 1	Reg. 2	Reg. 3	Reg. 4	Reg. 5	Reg. 6	Reg. 7
Region name	RNC	RNI	RSC	RSI	RSIM	REI	RWC
Population share (%)	5.52	17.52	21.41	16.74	6.52	6.69	25.60
Population change (%)	30.91	5.33	8.84	−14.41	−12.90	−11.90	−15.27

Note: The population share is based on the population estimates for 2005.
Abbreviations: C, coastal; E, eastern; I, inner (continental); M, mountainous; N, northern; R, region; S, southern; W, western.

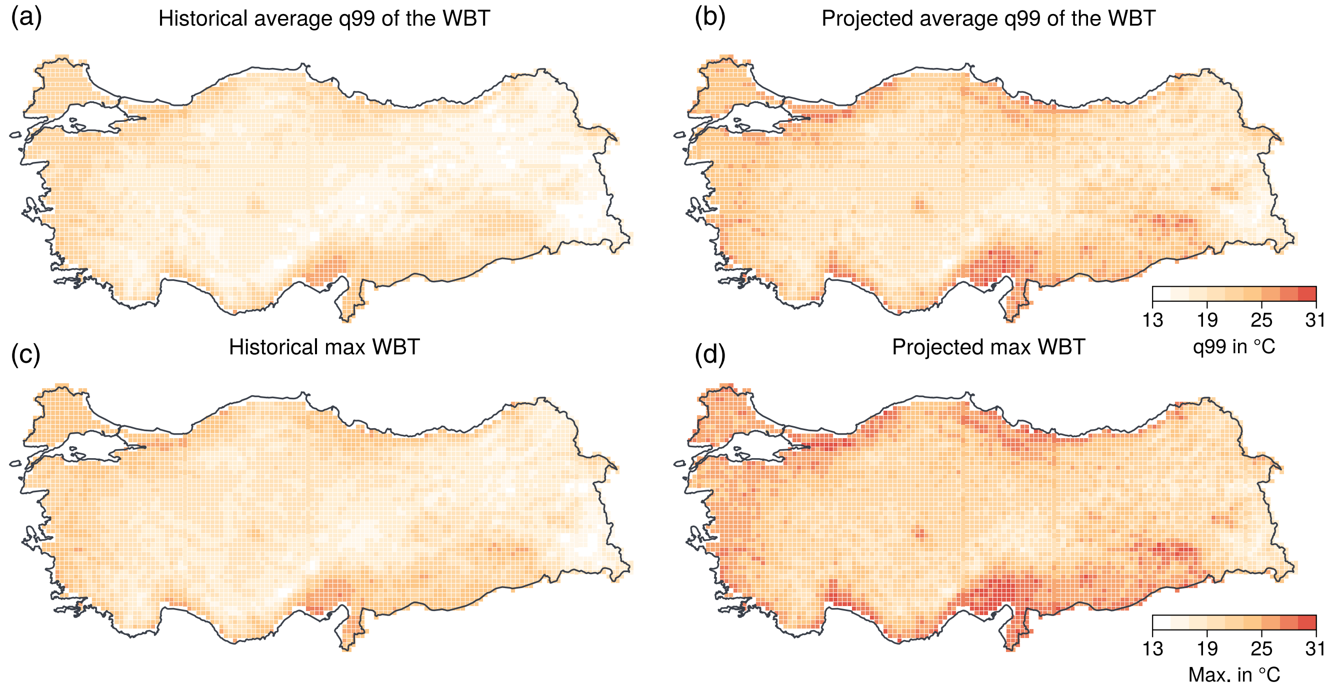

FIGURE 3 The average annual q99 (a, b) and max (c, d) values of the wet-bulb temperature (WBT) in degrees Celsius for each grid in the historical (a–c) and projection (b–d) periods. The average annual values were computed by calculating the q99 and max for every year in the corresponding historical and projection periods and then averaging them across the respective periods.

and 2 m relative humidity model outputs against the WBT derived from the ERA5-Land reanalysis for the 1985–2005 base period. Overall, the bias-correction approach we utilize performs well in representing the base period conditions for the WBT variable as portrayed by the ERA5-Land reanalysis data. The readers are referred to Data S1, Supporting Information for an in-depth validation of the model output.

3.2 | Anticipated changes in intensity and frequency of humid heat extremes

We first evaluate the country-wide humid heat stress extremes, characterized by the WBT, in the historical period, as well as the projected changes in their intensity, absolute frequency and relative frequency. Figure 3 shows the average annual 99th quantile (q99) and maximum (max) values of the WBT for each grid in the historical period and the projected changes in these values. Our results (b–d) suggest pronounced increase in q99 and max values across the majority of the country, especially along the coasts, relative to the historical period. This is evident by the q99 values in the projected period surpassing 29°C in some regions, compared to the q99 values in the historical period capped by the severe heat stress threshold of 27°C (Figure 3a). A model bias of less than 0.5°C for q99 against the ERA5-Land over the majority of the country in the historical period highlights the importance of these changes (Figure S5b). Further, the average annual max values are also expected to follow a similar increasing pattern in the projection period. Although

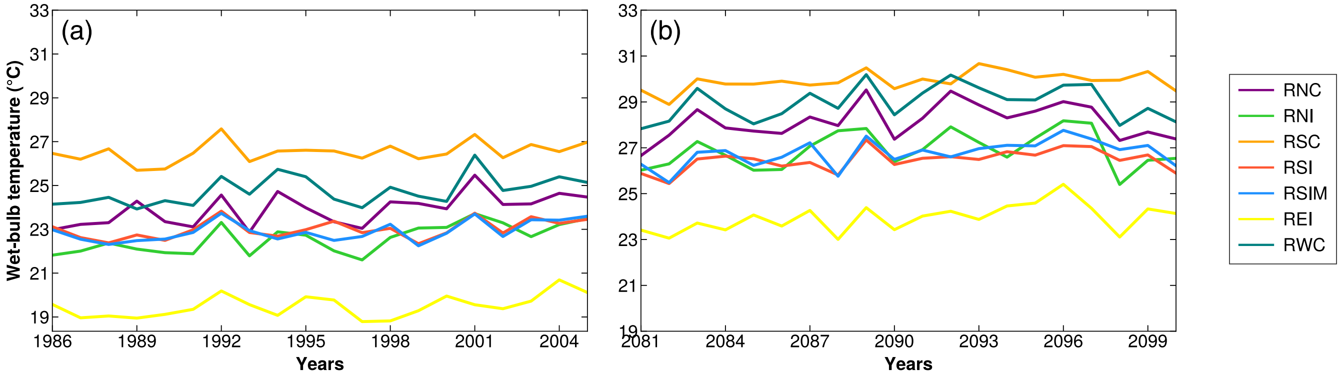

FIGURE 4 The regional maximum of the q99 values simulated during the historical (a) and projection (b) periods for each conceptualized *K*-means region. Each region is colour-coded, and readers can refer to Table 2 for a detailed description of these regions.

these values rarely exceed 27°C in the historical period (Figure 3c), there could be an increase by as much as 4°C in the projection period, approaching the dangerous heat stress threshold of 31°C. The all-time max in the country exceeds 33.8°C, an almost deadly WBT threshold. Most changes are concentrated along an elongated portion of the coastal areas of Turkey. Nevertheless, epicentres of the increase in extremes coincide with lower topography and can be clustered as follows: an array of cities east of the Marmara Sea, including Kocaeli, Sakarya, Duzce and Zonguldak; Izmir and Aydin on the Aegean coast; Antalya, Adana and Hatay on the Mediterranean coast; Samsun and Ordu on the Black Sea coast; Diyarbakir and Sanliurfa to southeast Turkey (Figure S1).

As can be seen in Figure 4, the surge in q99 values in the projection period is also evident for the conceptualized *K*-means regions. Both in the historical and projection periods, the highest WBT values are present in RSC and RWC, which constitute 21.41% and 25.60% of the total population in Turkey, respectively (Table 2). The lowest regional q99 values are seen in REI, located in the eastern parts of the country. While the regional maximum q99 values are mostly constrained to the 27°C threshold in the historical period, they occasionally exceed 30°C in the projection period, with these values hovering around the 26–27°C thresholds over most of the conceptualized *K*-means regions. This is further supported by the regional maximum q99 values in almost every *K*-means region, except for RSC and RSI, that experience statistically significant increasing trends in the historical period at the significance level of 95%.

We further evaluate frequency metrics that are derived from the WBT and based on absolute and relative heat stress thresholds. Prolonged exposure to threatening humid heat stress for a number of successive hours could increase the risks of illnesses and deaths (Sherwood & Huber, 2010). This qualifies it as a relevant metric to be considered in our analysis. Moreover, we differentiate between the absolute and relative frequency metrics because even if a region does not experience severe absolute humid heat extremes (e.g., 27°C), the magnitude of the change in local relative extremes (as characterized by higher quantiles such as q99) can still signal significant changes in the climate of the region.

Our findings show that while the NOD27 and NOCH27 are geographically constrained to the city of Adana in the historical period (Figure 5a–c), they encompass a geographically wide area in the projected period with dramatic increases in their magnitudes, with increases as much as 45 days for the NOD27 and 12 h for the NOCH27 (Figure 5b–d). Considering the bias in NOD27 of mainly less than 2 days over the city of Adana, the projected changes in these frequency metrics are significant. The regions with the greatest rise in the NOD27 and NOCH27 coincide with the cluster of areas in Figure 3, communicating the higher likelihood of humid heat extremes reigning within these locations. Over most of these clustered regions, almost a month every year is expected to experience severe humid heat stress, though not consecutively. Unlike the NOD27, the NOCH27 expresses the consecutive nature of heat stress, and the change in this metric relative to the historical period reaches half a day (i.e., 12 h). Particularly, the city of Adana is projected to be dominated by 10 h of severe humid heat stress in succession.

Some other regions, including the south of the Marmara Sea and the northwestern and southeastern edges of the country, are also subject to a rise in NOD27 and NOCH27, though less in magnitude than anticipated for the clustered regions. However, these regions with a slight increase in absolute frequency of the WBT extremes experience some of the greatest increases in the relative frequency metric of NOCHQ99 suggesting increased soil moisture deficit (Figure 5e,f). The surge in

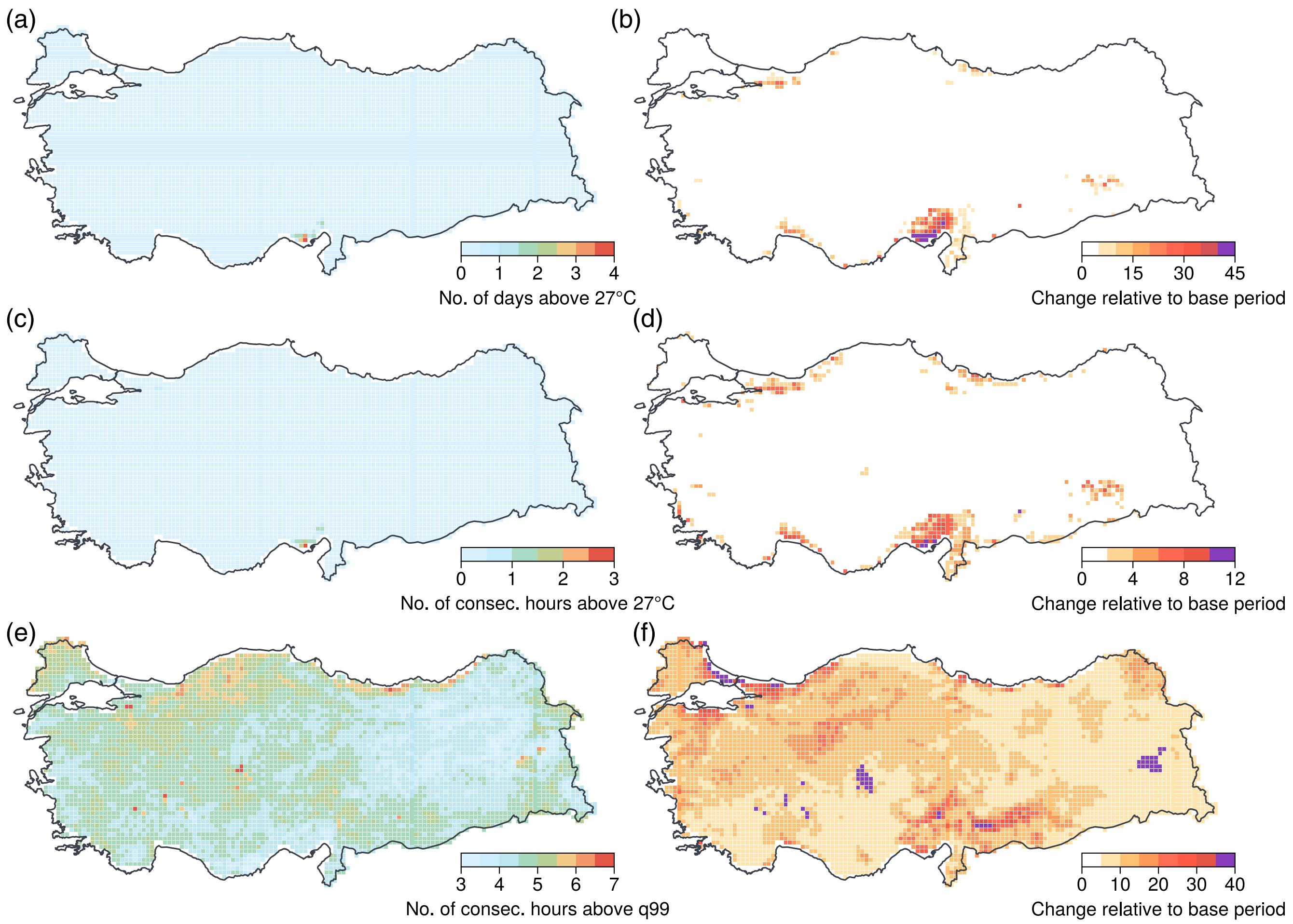

FIGURE 5 The historical period conditions (a, c, e) and projected changes (b, d, f) in the employed frequency metrics for humid heat extremes. These metrics are NOD27 (a, b; the number of days above 27°C), NOCH27 (c, d; the number of consecutive hours above 27°C), and NOCHQ99 (e, f; the number of consecutive hours above the local q99). The units are the same for each historical-projection period combination. The historical period q99 values are used to calculate the relative change in the projection period in (f).

NOCHQ99 values in the projection period is also notable for the surrounding of the most populated cities in Turkey, Istanbul and Ankara. It should be emphasized that although the coastal areas bear the burden of increase in the frequency of severe humid heat stress, a wider geographical area across the country, roughly 56% of the land area, is expected to confront conditions of heat stress, similar to the upper tail of the historical-period for at least an additional 10 consecutive hours.

3.3 | Population exposure to humid heat extremes in Turkey

We first examine the population distribution in Turkey for 2005 and the average population for 2081–2100 and calculate the percentage change between these periods (Figure 6). Overall, in the projection period, the population amount over many of the city centres is redistributed to populate their surroundings, thus reducing the population intensity in these regions, which include most of the cities enlisted in the clustered regions expected to experience a dramatic increase in severe humid heat stress (Figure 3). Therefore, consideration of the temporally evolving interaction between population amount and humid heat stress is crucial for quantifying population exposure.

Figure 7 illustrates the population exposure in the historical period, together with projected changes in the total population exposure and its components. The unit for the population exposure in our analysis is person-days, communicating the average number of people in a year that encounters severe humid heat stress with a daily maximum temperature of 27°C over a number of days. Consistent with the spatial distribution of the frequency and magnitude of severe humid heat stress in the

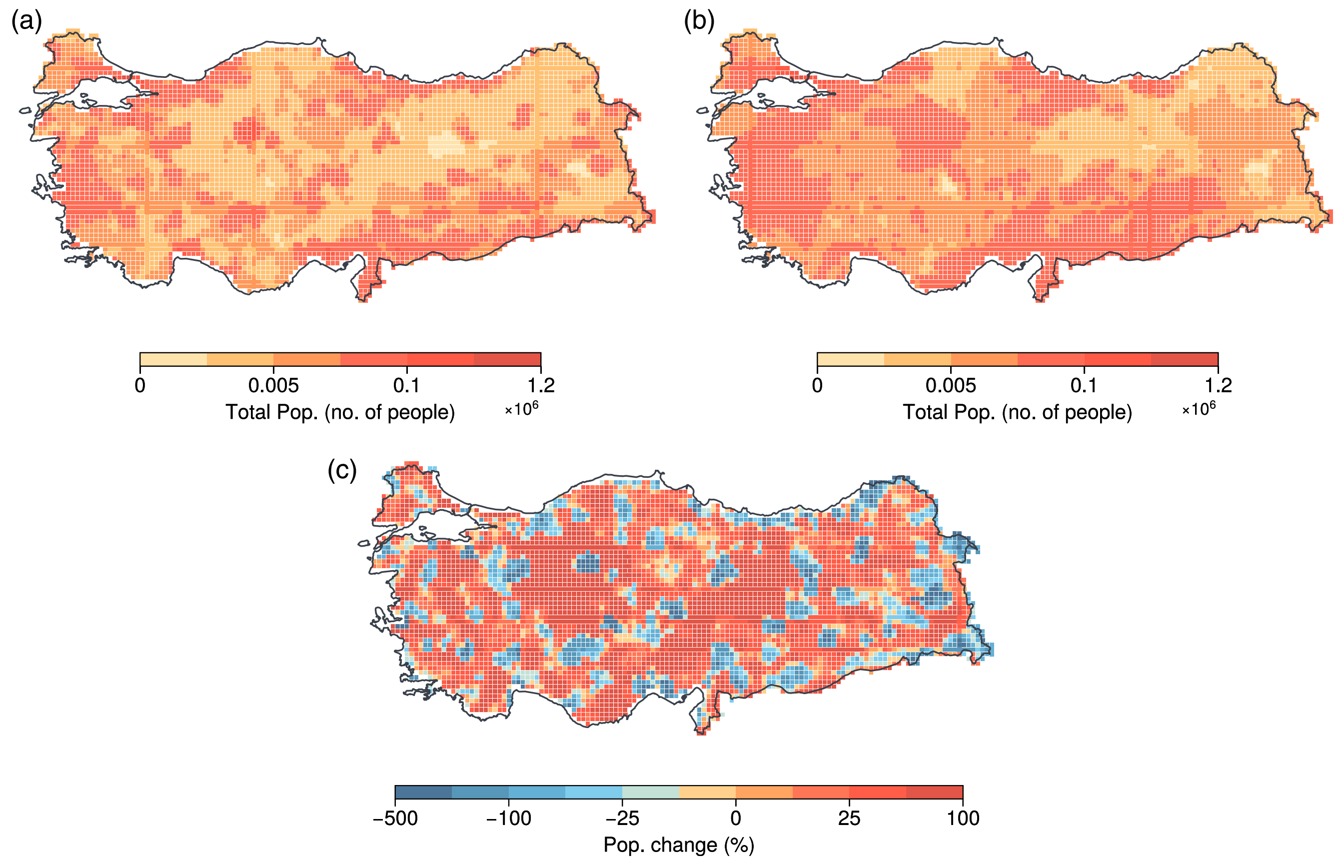

FIGURE 6 The total number of people at each grid during the historical (a) and projection (b) periods, along with the corresponding percentage change in population between these periods (c). We used the year 2005 to represent the historical period (GPWv4 data) and the average population amount to represent the projection period, specifically the average for the 2081–2100 period (SSP5 population estimates).

historical period, the exposure to such conditions is limited to specific geographic areas during the same period. The population exposed to these conditions is mainly located in the southeastern city of Adana and east of the Marmara Sea. The exposure to severe humid heat stress rarely exceeds 1 million person-days. In contrast, in the projection period, the total population exposure increases by at least 5000 person-days along most of the coastal locations, with a spatially intermittent surge in exposure by as much as 1.6 million person-days along this coastal line (Figure 7d). The areas with a surge in exposure to severe humid heat stress coincide with the cluster of regions emphasized in the intensity and frequency analysis (section 3.2). These clusters include the surroundings of Adana, Antalya, Izmir, Sakarya, Ordu and Diyarbakir. Our findings suggest that the population living close to coastal areas is particularly vulnerable to severe humid heat stress on a yearly basis. Exposure to these extremes occurring in the inland continental regions of the country is sporadic, with projections showing less pronounced increases. The population in far eastern Turkey is almost entirely spared from exposure to severe humid heat stress. We again stress that cities accommodating millions of people, including Istanbul and Izmir, experience the greatest increase in exposure. This is in spite of the finding that the majority of these cities will lose some of their population to their surroundings (Figure 6).

We further focus on the climate and population components of the total exposure (Figure 7b,c). These components can be interpreted as “the change in exposure if the climate of Turkey evolved in the future with the population remaining the same as 2005” and “the change in exposure if the climate remained the same as the average of the last five years in the historical period with the population evolving in the future.”

In a scenario where the only evolving component of the population exposure is the climate (Figure 7b), the immediate surrounding of Adana, Antalya, Diyarbakir and Sakarya would see an increase in exposure relative to the total population exposure (Figure 7d). For example, Adana would see an increase of as much as 6 million person-days. The cities of Antalya and Sakarya would see an increase of at least 1 million person-days, though the geographical scope of these increases is limited. An

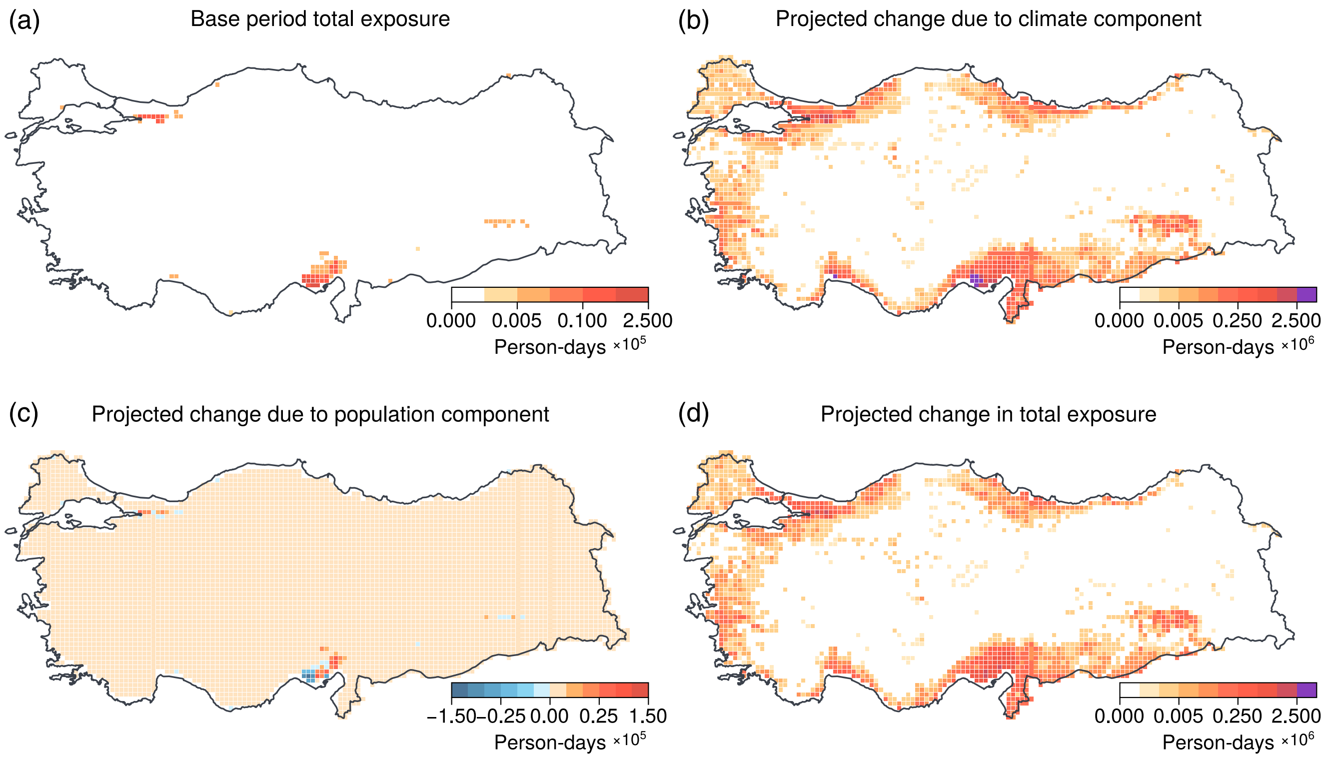

FIGURE 7 The total population exposure to severe humid heat stress (27°C) during the historical period (a) and the projected changes in the total population exposure (d), along with its climate (b) and population components (c). The population estimates for the year 2005 (the average of 2081–2100) were used for the calculation of exposure during the historical (projection) period. The units are in person-days, representing the number of people multiplied by the number of days in a year where the daily maximum wet-bulb temperature is above 27°C. The climate and population components of exposure can be understood as the following: "the alteration in exposure if Turkey's climate progresses into the future while maintaining the population of 2005" and "the alteration in exposure if the climate remains at the average of the last five years in the historical period while the population advances into the future."

increase of up to 500,000 person-days would be seen across the city of Diyarbakir. In contrast, some regions, including the west of Sakarya and the north of Adana, would see a decrease in exposure in the range of 500,000–1 million person-days. These changes in the climate component of the exposure compared to the changes in the total population exposure are provided by the projected increase and decrease in population from the last year of the historical period to the projection period. On the other hand, in a scenario where the only evolving component of the population exposure is the population (Figure 7c), the geographical extent of the exposure would be almost no different than that in the historical period exposure (Figure 7a). And the projected changes in exposure would be roughly one order of magnitude less than that for the total exposure, with a maximum exposure change of about 200,000 person-days in the city of Adana.

Humid heat stress not only intensifies over Turkey in the projections, but it also becomes more likely to occur in succession on an hourly basis, a condition associated with increased morbidity and mortality risk. This highlights the need to quantify the size of the population at risk of experiencing threatening heat stress conditions for multiple consecutive hours. Figure 8 displays the percentage of the total population in Turkey that is expected to experience three different humid heat stress thresholds (i.e., 27, 29 and 31°C) for various consecutive hours. To calculate this percentage, we used an algorithm to retrieve the persistence index, defined as the maximum number of consecutive hours above the WBT thresholds at every grid in our domain. We performed the same persistence index calculation for every year in the projection period. From this, we obtained both the temporal average and maximum values of the yearly persistence index. Finally, we divided the average population amount (i.e., 2081–2100 average) aggregated across grids that satisfied a threshold and consecutive hour criteria with the average total population amount to obtain the percentage. The solid and dashed lines in Figure 8 represent the temporal average and the temporal maximum of the yearly persistence index, respectively. The dashed lines illustrate a worst-case scenario.

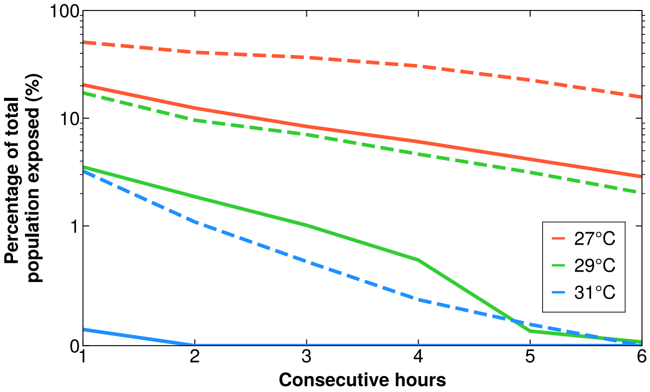

FIGURE 8 The percentage of Turkey's population that is anticipated to be exposed to three humid heat stress thresholds (27, 29 and 31°C) during a period of various consecutive hours. The solid and dashed lines illustrate the temporal average and the temporal maximum of the yearly persistence index, defined as the highest number of consecutive hours above the utilized wet-bulb temperature criteria for each grid in our domain.

Overall, we see a gradual decrease in the exposed percentage with an increase in consecutive hours. While, on average, 20.4% of the total population is exposed to 27°C and above for at least 1 h, only 4.15% of the total population is projected to experience this severe heat stress for five consecutive hours. These percentages correspond to roughly 13 million and 3 million people with respect to the mean projected population amount, respectively. Further, 3.5% of the total population is expected to experience 29°C and above, while this percentage is limited to 0.12% for at least five consecutive hours. Our projections suggest that the dangerous humid heat stress threshold of 31°C might be experienced by only 0.13% of the total population for at most one consecutive hour. It should be noted that 0.13% of the total population corresponds to more than 80 thousand people. Interestingly, as part of the worst-case scenario, more than half of the population is exposed to severe humid heat stress (i.e., 27°C) for at least 1 h, with this value reducing to 22.5% for six consecutive hours. The percentage of people that hypothetically might experience dangerous humid heat stress (i.e., 31°C) for five consecutive hours is 0.17%, still higher than the average exposed percentage to this threshold for at least 1 h. The remarkable detail is that the line for the hypothetical worst-case scenario for a higher humid heat stress threshold closely follows the line of its lower threshold counterpart.

3.4 | Regional aspects of population exposure in Turkey

A nationwide look at the projected exposure to summertime humid heat extremes depicts that these extremes are predominantly clustered along the western, northern and southern peripheries of the country, though the magnitude of exposure varies within these regions. Moreover, both the humid heat extremes and the population amount across the country exhibit annual variability. Considering these, we elaborate on the regional variability in total population exposure to two WBT thresholds (i.e., 27 and 29°C) for each year in the historical and projected periods (Figures 9 and 10). The regional mean and maximum of the population exposure are shown in Figures 9 and 10, respectively, and the colours in the figures correspond to the conceptualized *K*-means regions (Figure 2 and Table 2). In each figure, (a) and (b) subfigures correspond to the yearly exposure to the severe humid heat stress threshold of 27°C for the historical and projection periods, respectively, while subfigure (c) represents the yearly exposure to the 29°C threshold during the projection period.

First, there are no clear trends individually in the historical and projected time frames. However, there is a substantial rise in the regional mean population exposure to humid heat stress, rising to almost two orders of magnitude, from the historical period to the projection period. This is particularly noticeable in RSC, RWC and RNC, as shown in Figure 9. For example, while the mean exposure to severe humid heat stress for RWC is less than 3000 person-days in the historical period, it exceeds 100,000 person-days in 2 years in the projection period, with a minimum mean exposure of about three times the maximum mean exposure in the historical period. A similar change is also evident in RSC. Second, the mean exposure to the 29°C threshold in the projection period in RSC, RWC and RNC is, interestingly, greater than the corresponding mean exposure to 27°C in the historical period. RWC, in particular, is subject to maximum mean exposure to 29°C up to seven times the maximum mean exposure to 27°C in the historical period. In addition, while the mean exposure to 27°C in RNC is predominantly close to zero during the historical period, the mean exposure to 29°C in the same region occasionally exceeds 2500 person-days in the projection period.

The regional maximum population exposure also experiences a surge between the historical and projected periods, with the increase reaching one order of magnitude in some years (Figure 10). RSC and RWC are again the regions with the highest total population exposure, followed by RNC. However, it is RWC that is subject to the greatest increase in maximum regional exposure. Namely, though RSC dominates in the maximum exposure to severe humid heat stress in the historical period, RWC takes the lead in the projection period, confronting a total population exposure of as much as 3 million person-days (Figure 10b). The maximum exposure to

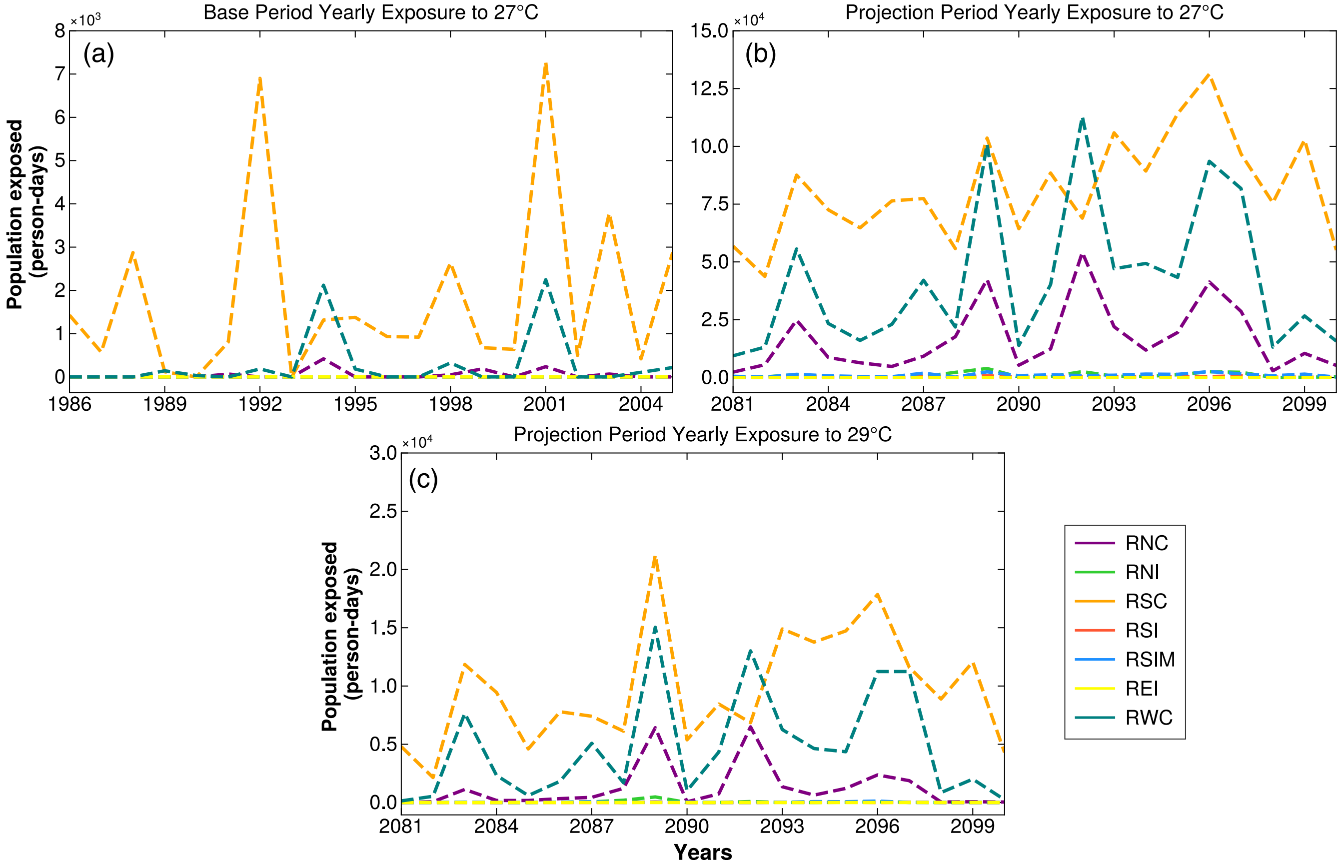

FIGURE 9 Regional-mean yearly exposure to 27°C (severe humid heat stress) in the historical (a) and projection periods (b), along with regional-mean yearly exposure to 29°C only during the projection period (c). The exposure values are shown in the person-days unit. The conceptualized *K*-means regions are represented with different colours, consistent with the colours in Figure 2.

27°C in the same period in RSC oscillates about the 1 million person-days threshold. Additionally, it should be noted that the *K*-means regions that are situated across the inner continental parts of the country (i.e., RNI, RSI and RSIM) also encounter maximum exposure to severe humid heat stress of up to 100,000 person-days in the projection period (Figure 10b,c), whereas this was not the case for the projected regional mean exposure (Figure 9b,c).

4 | DISCUSSION

Our results accentuate the surge in humid heat extremes and the consequent population exposure to these conditions, particularly along the coastal areas of Turkey. This is accompanied by an observed increase in warm spell duration and a projected increase in surface temperatures by as much as 5°C, primarily in regions with coastal characteristics (Onol & Unal, 2014; Toros et al., 2019). Our findings carry significant implications for society and a wide range of sectors, including the economy and tourism. Namely, the vast majority of the population in the country resides in proximity to coastal locations, rendering those with pre-existing health problems or limited access to cooling systems more susceptible to the adverse impacts of humid heat stress. Further, studies suggest a reduction in labour productivity due to the direct exposure of outdoor workers to heat stress conditions (Dunne et al., 2013), thereby indirectly affecting overall economic productivity.

Our projections indicate that individuals will not only experience intensified humid heat stress but will also face prolonged exposure to such conditions for several hours in succession. Speizer et al. (2022) showed that day-to-day clustering of humid heat extremes is possible in some regions. This finding, along with ours, can serve as a proxy for predicting the likelihood of an hour with humid heat extreme occurrence being followed by another. Further, it is well established in the literature that morbidity and mortality become more likely with exposure to humid heat extremes for many consecutive hours (Buzan & Huber, 2020). Notably, a more comprehensive analysis would consider quantifying population

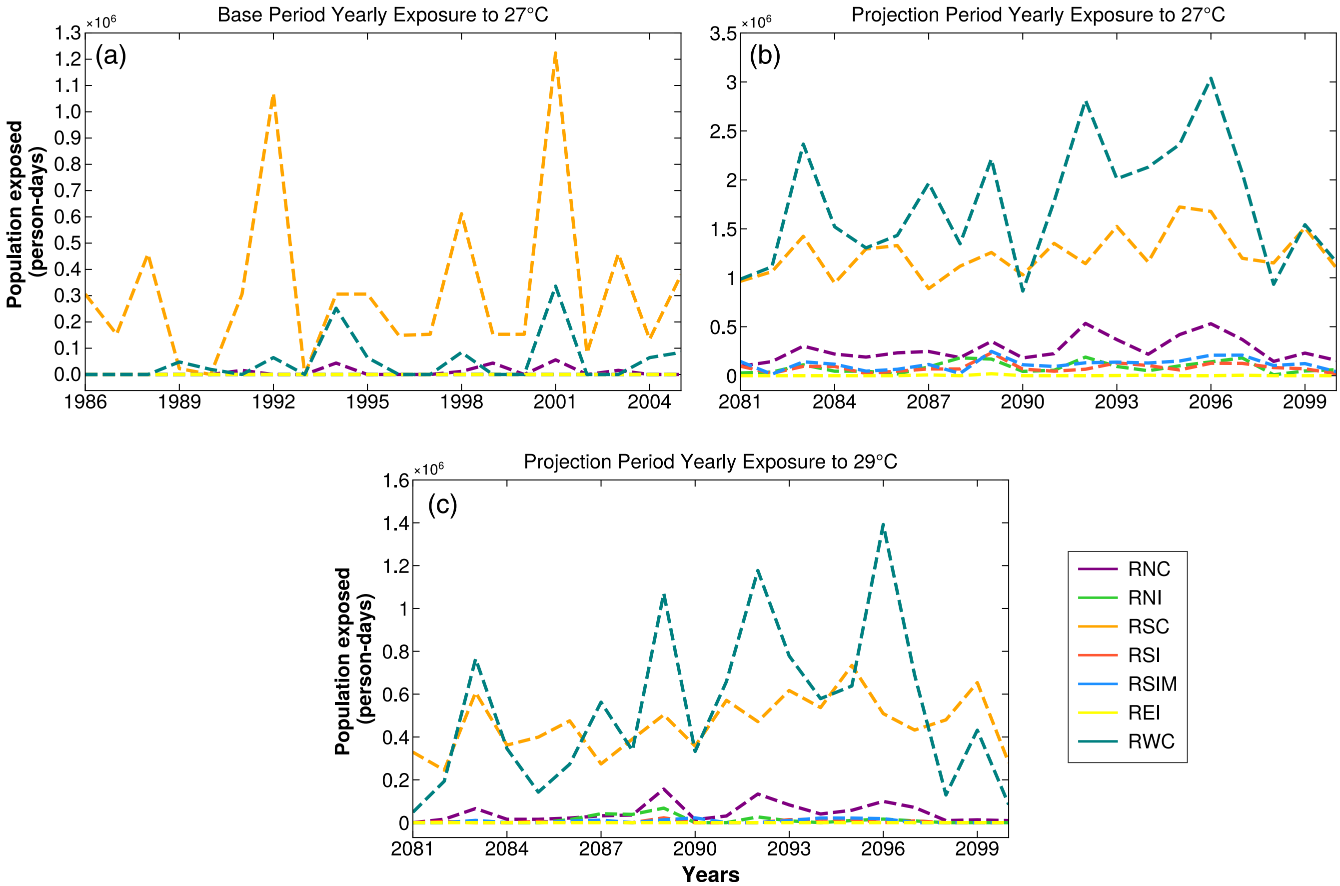

FIGURE 10 Regional-maximum yearly exposure to 27°C (severe humid heat stress) in the historical (a) and projection periods (b), along with regional-maximum yearly exposure to 29°C only during the projection period (c). The exposure values are shown in the person-days unit. The conceptualized *K*-means regions are represented with different colours, consistent with the colours in Figure 2.

exposure to heat stress taking into account various socio-economic and demographic characteristics, including but not limited to different age groups, income levels, literacy and underlying health conditions.

We demonstrate the regions in Turkey that are most susceptible to dangerous humid heat extremes and to what extent the population will confront these extremes, informing the decision-makers about the cluster of regions that needs particular focus in terms of mitigation and adaptation. While most research focuses on the global aspects of humid heat extremes and population exposure, greater attention should be directed toward the regional aspects (Batibeniz et al., 2020; Rogers et al., 2021). This is particularly important since countries might have different methods of coping with heat stress in different regions. Our results suggest that while the epicentre of the changes in the intensity and frequency of dry heat is rather wider geography spanning the eastern and western portions of the country (Onol & Unal, 2014; Sen et al., 2012), the corresponding changes in humid heat are more localized, such as in the surrounding of Adana and Sakarya. Despite the dissimilarities in climate between these cities, they share two vital features: proximity to a water resource and low topography. We argue that, in addition to synoptic-scale forcings, these characteristics are pivotal in shaping the spatial distribution of humid heat extremes. We do not dive into the large-scale synoptic conditions that are conducive to these extremes in Turkey. However, this should be prioritized in future work, as it is shown in the literature that there is a variety of meteorological conditions that can promote humid heat extremes in a region modulated by local and regional factors, such as topography, land use/land cover, and irrigation regimes (Raymond et al., 2017, 2020). Although we are unable to make direct comparison with the outcomes of other humid heat stress studies, our results are consistent with the finding that coastal Middle Eastern locations are more prone to confront humid heat stress (Raymond et al., 2020), and it is these coastal regions that are projected to experience the largest increase in humid heat across the country, similar to what Diffenbaugh et al. (2007) argue. Our study provides a benefit to the modelling community in the sense that we show the reproducibility of the reference-period humid heat conditions over one of the countries susceptible to these conditions the most. This is further critical given that the majority of the regional studies leans toward the use of a reanalysis, and evaluating the model performance against reanalysis should be prioritized for regional humid heat stress studies (Mishra et al., 2020).

Here, the urbanization impact, which we cannot account for in our study given our model resolution, should be incorporated into our understanding as a vital factor that can further restructure the spatial and temporal characteristics of humid heat stress. Urbanized regions promote the well-established urban heat island effect, which becomes more prominent at night (Oke et al., 2017). Thus, greater temperature values over urban areas, occasionally coincident with high-humidity conditions, can exacerbate humid heat extremes, especially at night. It should also be noted that urban surfaces can act to reduce humidity over urban regions (Meili et al., 2022), compensating for the increase in humid heat stress due to temperature increase (Coffel et al., 2019). Again, our results can not explicitly account for the urbanization-induced changes in humid heat stress. Using convection-resolving scale simulations coupled with urban canopy layer models will not only facilitate a better understanding of local circulations triggered by urban surfaces but also provide the researchers with an environment to test the sensitivity of humid heat stress to these local circulations.

Our findings align with the expected humid heat stress conditions in a future where significant measures to curb CO_2 emissions are not taken. However, studies emphasize that the range of dry heat conditions in Turkey can vary dramatically across the spectrum of the different emission scenarios (Demircan et al., 2017). The same comparison should also be made for the humid heat extremes in Turkey since our findings of exposure to these extremes likely represent the worst-case scenario. Another limitation of our study is that we cannot quantify uncertainty in humid heat stress exposure. This is because our results are based on the simulations that use a single initial-boundary condition data. This limitation can be overcome by using an ensemble of simulations, which incurs a high computational cost, particularly at convection-resolving scales.

Finally, we use the wet-bulb temperature as our humid heat stress metric, while a variety of other metrics can be employed for the same purpose, including the Heat Index (Anderson et al., 2013) and Wet-Bulb Globe Temperature (Willett & Sherwood, 2012). Given the sensitive nature of heat stress magnitude and pattern to the employed metric (Freychet et al., 2022; Tuholske et al., 2021), we reiterate the importance of metric comparison studies for Turkey that can robustify our conclusions. Nevertheless, we still argue that the overall pattern of humid heat stress extremes and population exposure across Turkey would look similar regardless of the used metric and concentrate along most of the coastal regions.

5 | CONCLUSION

In this study, we elaborate on the anticipated changes in the frequency and intensity of humid heat extremes and the population exposure to these extremes in Turkey between the defined historical and projection periods. To address this issue, we run long-term simulations using the COSMO-CLM model and employ the wet-bulb temperature, more accurately reflects the effect of climate on human health, as our heat stress metric derived from the surface temperature and relative humidity model outputs. We communicate not only the nationwide changes in the pattern and magnitude of humid heat stress and exposure but also regional aspects of it, conceptualizing *K*-means regions. The conclusions are as follows.

First, the intensity of humid heat extremes increases dramatically across the country. The average annual q99 of wet-bulb temperature experiences an increase by more than 2°C exceeding 29°C in some regions in the projection period, with the all-time maximum reaching 33.8°C, an almost deadly threshold.

Second, similar changes are also revealed for the frequency of humid heat stress. The most significant increase in NOD27 and NOCH27 during the projection period is seen over the cluster of regions, which include the surroundings of Adana, Antalya, Izmir, Sakarya, Ordu and Diyarbakir, most of which are coastal locations. Nearly 1 month per year is anticipated to experience severe humid heat stress over these clustered regions, though not consecutively. Specifically, our projections indicate that the city of Adana will experience severe humid heat stress lasting for 10 consecutive hours, and approximately 56% of the land area across the country will face a local upper tail of heat stress conditions for at least an extra 10 consecutive hours during the projection period.

Finally, despite the projected population loss of cities to their surroundings, we highlight a surge in total population exposure to humid heat stress along most coastal regions by as much as 1.6 million person-days, which we mainly attribute to the change in the climate similar to Freychet et al. (2022). During the historical period, in contrast, the exposed population is constrained to the surrounding of Adana and east of the Marmara Sea, with exposure seldom exceeding 1 million person-days. From a regional perspective, the population residing in the RSC, RWC and RNC regions is expected to confront the highest levels of exposure to humid heat stress. Remarkably, these regions are mainly located along the coast, except for the far eastern parts of the RSC region. Additionally, our analysis suggests that more than 20% of the total population in Turkey can experience severe humid heat stress for at least 1 h, with this number reduced to 4.15% for at least five consecutive hours. Therefore, national mitigation strategies should be established to address the impacts of humid heat stress in these regions. This is especially important for individuals working in direct sunlight, those with limited access to air-conditioning, healthcare services, emergency medical care as well as the homeless, elderly populations and individuals particularly those suffering from specific health conditions.

AUTHOR CONTRIBUTIONS

Berkay Donmez: Conceptualization; methodology; software; data curation; formal analysis; validation; visualization; investigation; writing – original draft; writing – review and editing. **Kutay Donmez:** Methodology; software; data curation; investigation; validation; formal analysis; visualization; writing – review and editing; writing – original draft. **Cemre Yürük Sonuç:** Conceptualization; methodology; funding acquisition; writing – review and editing; resources. **Yurdanur Unal:** Conceptualization; methodology; writing – review and editing; resources; supervision; funding acquisition; project administration.

ACKNOWLEDGEMENTS

We would like to thank the National Center for High-Performance Computing (UHeM) for providing us with supercomputing. This work is supported by TUBITAK project grant number 114Y047 under the European Union's Seventh Framework Programme ERAfrica LOCLIM3.

CONFLICT OF INTEREST STATEMENT

The authors declare no conflicts of interest.

DATA AVAILABILITY STATEMENT

The data that support the findings of this study are available from the corresponding author upon reasonable request.

ORCID

Berkay Donmez https://orcid.org/0000-0001-5978-3642
Kutay Donmez https://orcid.org/0000-0003-2344-5822
Cemre Yürük Sonuç https://orcid.org/0000-0002-8585-1319
Yurdanur Unal https://orcid.org/0000-0003-2006-1372

REFERENCES

Ahmadalipour, A., Moradkhani, H. & Kumar, M. (2019) Mortality risk from heat stress expected to hit poorest nations the hardest. *Climatic Change*, 152, 569–579. Available from: https://doi.org/10.1088/1748-9326/ac69fc

Anderson, G. B., Bell, M. L., & Peng, R. D. (2013). Methods to Calculate the Heat Index as an Exposure Metric in Environmental Health Research. *Environmental Health Perspectives*, 121(10), 1111–1119. https://doi.org/10.1289/ehp.1206273

Batibeniz, F., Ashfaq, M., Diffenbaugh, N.S., Key, K., Evans, K.J., Turuncoglu, U.U. et al. (2020) Doubling of U.S. population exposure to climate extremes by 2050. *Earth's Futures*, 8, e2019EF001421. Available from: https://doi.org/10.1029/2019EF001421

Buzan, J.R. & Huber, M. (2020) Moist heat stress on a hotter earth. *Annual Review of Earth and Planetary Sciences*, 48(1), 623–655. Available from: https://doi.org/10.1146/annurev-earth-053018-060100

Chen, H., He, W., Sun, J. & Chen, L. (2022) Increases of extreme heat-humidity days endanger future populations living in China. *Environmental Research Letters*, 17, 064013. Available from: https://doi.org/10.1088/1748-9326/ac69fc

CIESIN (Center for International Earth Science Information Network-Columbia University). (2018) *Gridded population of the world, version 4 (GPWv4), population count, revision 11*. Palisades, NY: NASA Socioeconomic Data and Applications Center. Available from: https://doi.org/10.7927/H4JW8BX5

Coffel, E.D., Horton, R.M., Winter, J.M. & Mankin, J.S. (2019) Nonlinear increases in extreme temperatures paradoxically dampen increases in extreme humid-heat. *Environmental Research Letters*, 14, 084003. Available from: https://doi.org/10.1088/1748-9326/ab28b7

Demircan, M., Gurkan, H., Eskioglu, O., Arabaci, H. & Coskun, M. (2017) Climate change projections for Turkey: three models and two scenarios. *Turkish Journal of Water Science and Management*, 1(1), 22–43. Available from: https://doi.org/10.31807/tjwsm.297183

Diffenbaugh, N.S., Pal, J.S., Giorgi, F. & Gao, X. (2007) Heat stress intensification in the Mediterranean climate change hotspot. *Geophysical Research Letters*, 34, L11706. Available from: https://doi.org/10.1029/2007GL030000

Dunne, J.P., Stouffer, R.J. & John, J.G. (2013) Reductions in labour capacity from heat stress under climate warming. *Nature Climate Change*, 3, 563–566. Available from: https://doi.org/10.1038/nclimate1827

Fischer, E.M. & Knutti, R. (2013) Robust projections of combined humidity and temperature extremes. *Nature Climate Change*, 3, 126–130. Available from: https://doi.org/10.1038/nclimate1682

Freychet, N., Hegerl, G.C., Lord, N.S., Lo, Y.T.E., Mitchell, D. & Collins, M. (2022) Robust increase in population exposure to heat stress with increasing global warming. *Environmental Research Letters*, 17, 064049. Available from: https://doi.org/10.1088/1748-9326/ac71b9

Gasper, R., Blohm, A. & Ruth, M. (2011) Social and economic impacts of climate change on the urban environment. *Current*

Opinion in Environment Sustainability, 3, 150–157. Available from: https://doi.org/10.1016/j.cosust.2010.12.009

Jones, B. & O'Neill, B.C. (2020) *Global one-eighth degree population base year and projection grids based on the shared socioeconomic pathways, revision 01*. Palisades, NY: NASA Socioeconomic Data and Applications Center (SEDAC). Available from: https://doi.org/10.7927/m30p-j498

Jones, B., O'Neill, B.C., McDaniel, L., McGinnis, S., Mearns, L.O. & Tebaldi, C. (2015) Future population exposure to US heat extremes. *Nature Climate Change*, 5, 652–655. Available from: https://doi.org/10.1038/nclimate2631

Kelebek, M.B., Batibeniz, F. & Onol, B. (2021) Exposure assessment of climate extremes over the Europe–Mediterranean region. *Atmosphere*, 12(5), 633. Available from: https://doi.org/10.3390/atmos12050633

Logan, T., Aoun, A., Bourgault, P., Dupuis, É., Huard, D., Lavoie, J. et al. (2023) Ouranosinc/xclim: v0.40.0. https://doi.org/10.5281/zenodo.7796479

Matthews, T.K.R., Wilby, R.L. & Murphy, C. (2017) Communicating the deadly consequences of global warming for human heat stress. *Proceedings of the National Academy of Sciences of the United States of America*, 114, 3861–3866. Available from: https://doi.org/10.1073/pnas.1617526114

Mazdiyasni, O., Aghakouchak, A., Davis, S.J., Madadgar, S., Mehran, A., Ragno, E. et al. (2017) Increasing probability of mortality during Indian heat waves. *Science Advances*, 3, e1700066. Available from: https://doi.org/10.1126/sciadv.1700066

Meili, N., Paschalis, A., Manoli, G. & Fatichi, S. (2022) Diurnal and seasonal patterns of global urban dry islands. *Environmental Research Letters*, 17, 054044. Available from: https://doi.org/10.1088/1748-9326/ac68f8

Mishra, V., Ambika, A.K., Asoka, A., Aadhar, S., Buzan, J., Kumar, R. et al. (2020) Moist heat stress extremes in India enhanced by irrigation. *Nature Geoscience*, 13, 722–728. Available from: https://doi.org/10.1038/s41561-020-00650-8

Mora, C., Dousset, B., Caldwell, I.R., Powell, F.E., Geronimo, R.C., Bielecki, C.R. et al. (2017) Global risk of deadly heat. *Nature Climate Change*, 7, 501–506. Available from: https://doi.org/10.1038/nclimate3322

Oke, T.R., Mills, G., Christen, A. & Voogt, J.A. (2017) *Urban climates*, Vol. 16. Cambridge: Cambridge University Press. Available from: https://doi.org/10.1017/9781139016476

Onol, B., Bozkurt, D., Turuncoglu, U.U., Sen, O.L. & Dalfes, H.N. (2014) Evaluation of the twenty-first century RCM simulations driven by multiple GCMs over the eastern Mediterranean–Black Sea region. *Climate Dynamics*, 42, 1949–1965. Available from: https://doi.org/10.1007/s00382-013-1966-7

Onol, B. & Unal, Y.S. (2014) Assessment of climate change simulations over climate zones of Turkey. *Regional Environmental Change*, 14, 1921–1935. Available from: https://doi.org/10.1007/s10113-012-0335-0

Raymond, C., Matthews, T. & Horton, R.M. (2020) The emergence of heat and humidity too severe for human tolerance. *Science Advances*, 6, 19. Available from: https://doi.org/10.1126/sciadv.aaw1838

Raymond, C., Matthews, T., Horton, R.M., Fischer, E.M., Fueglistaler, S., Ivanovich, C. et al. (2021) On the controlling factors for globally extreme humid heat. *Geophysical Research Letters*, 48, e2021GL096082. Available from: https://doi.org/10.1029/2021GL096082

Raymond, C., Singh, D. & Horton, R.M. (2017) Spatiotemporal patterns and synoptics of extreme wet-bulb temperature in the contiguous United States. *Journal of Geophysical Research: Atmospheres*, 122, 13108–13124. Available from: https://doi.org/10.1002/2017JD027140

Ritter, B., & Geleyn, J.-F. (1992). A Comprehensive Radiation Scheme for Numerical Weather Prediction Models with Potential Applications in Climate Simulations. *Monthly Weather Review*, 120(2), 303–325. https://doi.org/10.1175/1520-0493(1992)120<0303:acrsfn>2.0.co;2

Rogers, C.D.W., Ting, M., Li, C., Kornhuber, K., Coffel, E.D., Horton, R.M. et al. (2021) Recent increases in exposure to extreme humid-heat events disproportionately affect populated regions. *Geophysical Research Letters*, 48, e2021GL094183. Available from: https://doi.org/10.1029/2021GL094183

Rothfusz, L.P. (1990) *The heat index equation (or, more than you ever wanted to know about heat index)*. Forth Worth, TX: NWS S. Reg. Headquarters. Technical Attachment, SR/SSD 90-23. Available from: https://www.weather.gov/media/ffc/ta_htindx.PDF

Russo, S., Sillmann, J. & Sterl, A. (2017) Humid heat waves at different warming levels. *Scientific Reports*, 7, 7477. Available from: https://doi.org/10.1038/s41598-017-07536-7

Sarangi, C., Qian, Y., Li, J., Leung, L.R., Chakraborty, T.C. & Liu, Y. (2021) Urbanization amplifies nighttime heat stress on warmer days over the US. *Geophysical Research Letters*, 48, e2021GL095678. Available from: https://doi.org/10.1029/2021GL095678

Sen, B., Topcu, S., Turkes, M., Sen, B. & Warner, J.F. (2012) Projecting climate change, drought conditions and crop productivity in Turkey. *Climate Research*, 52, 175–191. Available from: https://doi.org/10.3354/cr01074

Sherwood, S.C. (2018) How important is humidity in heat stress? *Journal of Geophysical Research: Atmospheres*, 123, 11808–11810. Available from: https://doi.org/10.1029/2018JD028969

Sherwood, S.C. & Huber, M. (2010) An adaptability limit to climate change due to heat stress. *Proceedings of the National Academy of Sciences of the United States of America*, 107, 9552–9555. Available from: https://doi.org/10.1073/pnas.0913352107

Speizer, S., Raymond, C., Ivanovich, C. & Horton, R.M. (2022) Concentrated and intensifying humid heat extremes in the IPCC AR6 regions. *Geophysical Research Letters*, 49, 5. Available from: https://doi.org/10.1029/2021GL097261

Stull, R. (2011) Wet-bulb temperature from relative humidity and air temperature. *Journal of Applied Meteorology and Climatology*, 50, 2267–2269. Available from: https://doi.org/10.1175/JAMC-D-11-0143.1

Tiedtke, M. (1989). A Comprehensive Mass Flux Scheme for Cumulus Parameterization in Large-Scale Models. *Monthly Weather Review*, 117(8), 1779–1800. https://doi.org/10.1175/1520-0493(1989)117<1779:acmfsf>2.0.co;2

Toros, H., Mokari, M. & Abbasnia, M. (2019) Regional variability of temperature extremes in the maritime climate of Turkey: a case study to develop agricultural adaptation strategies under climate change. *Modeling Earth Systems and Environment*, 5, 857–865. Available from: https://doi.org/10.1007/s40808-019-00572-4

Tuholske, C., Caylor, K., Funk, C., Verdin, A., Sweeney, S., Grace, K. et al. (2021) Global urban population exposure to extreme heat. *Proceedings of the National Academy of Sciences of the United States of America*, 118(41), e2024792118. Available from: https://doi.org/10.1073/pnas.2024792118

Turkes, M. & Sumer, U.M. (2004) Spatial and temporal patterns of trends and variability in diurnal temperature ranges of Turkey. *Theoretical and Applied Climatology*, 77, 195–227. Available from: https://doi.org/10.1007/s00704-003-0024-5

Wang, P., Yang, Y., Tang, J., Leung, L.R. & Liao, H. (2021) Intensified humid heat events under global warming. *Geophysical Research Letters*, 48(2), e2020GL091462. Available from: https://doi.org/10.1029/2020GL091462

Willett, K.M. & Sherwood, S. (2012) Exceedance of heat index thresholds for 15 regions under a warming climate using the wet-bulb globe temperature. *International Journal of Climatology*, 32, 161–177. Available from: https://doi.org/10.1002/joc.2257

Wu, J., Zhou, Y., Gao, Y., Fu, J.S., Johnson, B.A., Huang, C. et al. (2014) Estimation and uncertainty analysis of impacts of future heat waves on mortality in the eastern United States. *Environmental Health Perspectives*, 122, 1–16. Available from: https://doi.org/10.1289/ehp.1306670

SUPPORTING INFORMATION

Additional supporting information can be found online in the Supporting Information section at the end of this article.

How to cite this article: Donmez, B., Donmez, K., Sonuç, C. Y., & Unal, Y. (2024). Future change of humid heat extremes and population exposure in Turkey. *International Journal of Climatology*, *44*(11), 3912–3929. https://doi.org/10.1002/joc.8559